cinoma and its incidence after interferon treatment in patients with chronic hepatitis C. Osaka Liver Disease Study Group. Hepatology 1998;27:1394–402.
13. Imai Y, Kawata S, Tamura S, Yabuuchi I, Noda S, Inada M, Maeda Y, et al. Relation of interferon therapy and hepatocellular carcinoma in patients with chronic hepatitis C. Osaka Hepatocellular Carcinoma Prevention Study Group. Ann Intern Med 1998;129:94–9.
14. Ikeda K, Saitoh S, Arase Y, Chayama K, Suzuki Y, Kobayashi M, Tsubota A, et al. Effect of interferon therapy on hepatocellular carcinogenesis in patients with chronic hepatitis type C: a long-term observation study of 1,643 patients using statistical bias correction with proportional hazard analysis. Hepatology 1999;29: 1124–30.
15. Yoshida H, Tateishi R, Arakawa Y, Sata M, Fujiyama S, Nishiguchi S, Ishibashi H, et al. Benefit of interferon therapy in hepatocellular carcinoma prevention for individual patients with chronic hepatitis C. Gut 2004;53:425–30.
16. Okanoue T, Minami M, Makiyama A, Sumida Y, Yasui K, Itoh Y. Natural course of asymptomatic hepatitis C virus-infected patients and hepatocellular carcinoma after interferon therapy. Clin Gastroenterol Hepatol 2005;3:S89–91.
17. Ikeda K, Marusawa H, Osaki Y, Nakamura T, Kitajima N, Yamashita Y, Kudo M, et al. Antibody to hepatitis B core antigen and risk for hepatitis C-related hepatocellular carcinoma: a prospective study. Ann Intern Med 2007;146:649–56.

ELSEVIER

Journal of Hepatology 50 (2009) 1236–1246

Journal of Hepatology

www.elsevier.com/locate/jhep

Polyenephosphatidylcholine prevents alcoholic liver disease in PPARα-null mice through attenuation of increases in oxidative stress☆

Wataru Okiyama[1,2,†], Naoki Tanaka[1,2,*,†], Tamie Nakajima[3], Eiji Tanaka[2], Kendo Kiyosawa[4], Frank J. Gonzalez[5], Toshifumi Aoyama[1]

[1]*Department of Metabolic Regulation, Institute on Aging and Adaptation, Shinshu University Graduate School of Medicine, Asahi 3-1-1, Matsumoto 390-8621, Japan*

[2]*Department of Gastroenterology, Shinshu University School of Medicine, Matsumoto, Japan*

[3]*Department of Occupational Environmental Health, Nagoya University Graduate School of Medicine, Nagoya, Japan*

[4]*Department of Internal Medicine, Nagano Red Cross Hospital, Nagano, Japan*

[5]*Laboratory of Metabolism, Center for Cancer Research, National Cancer Institute, National Institutes of Health, Bethesda, MD, USA*

***Background/Aims*: Alcoholic liver disease (ALD) is one of the leading causes of cirrhosis and yet efficient therapeutic strategies are lacking. Polyenephosphatidylcholine (PPC), a major component of essential phospholipids, prevented alcoholic liver fibrosis in baboons, but its precise mechanism remains uncertain. We aimed to explore the effects of PPC on ALD using ethanol-fed peroxisome proliferator-activated receptor α (*Ppara*)-null mice, showing several similarities to human ALD.**

***Methods*: Male wild-type and *Ppara*-null mice were pair-fed a Lieber-DeCarli control or 4% ethanol-containing diet with or without PPC (30 mg/kg/day) for 6 months.**

***Results*: PPC significantly ameliorated ethanol-induced hepatocyte damage and hepatitis in *Ppara*-null mice. These effects were likely a consequence of decreased oxidative stress through down-regulation of reactive oxygen species (ROS)-generating enzymes, including cytochrome P450 2E1, acyl-CoA oxidase, and NADPH oxidases, in addition to restoration of increases in Toll-like receptor 4 and CD14. PPC also decreased Bax and truncated Bid, thus inhibiting apoptosis. Furthermore, PPC suppressed increases in transforming growth factor-β1 expression and hepatic stellate cell activation, which retarded hepatic fibrogenesis.**

***Conclusions*: PPC exhibited anti-inflammatory, anti-apoptotic, and anti-fibrotic effects on ALD as a result of inhibition of the overexpression of ROS-generating enzymes. Our results demonstrate detailed molecular mechanisms of the antioxidant action of PPC.**

***Keywords*: Cytochrome P450 2E1; Acyl-CoA oxidase; NOX-4; MCP-1; TLR-4**

Received 8 December 2008; received in revised form 18 January 2009; accepted 27 January 2009; available online 2 April 2009

Associate Editor: C.P. Day

☆ The authors who have taken part in this study declared that they do not have anything to disclose regarding funding or conflict of interest with respect to this manuscript.

* Corresponding author. Fax: +81 263 37 3094.

E-mail address: naopi@shinshu-u.ac.jp (N. Tanaka).

† These authors contributed equally to this work.

Abbreviations: ADH, alcohol dehydrogenase; ALDH, aldehyde dehydrogenase; AOX, acyl-coenzyme A oxidase; AP-1, activator protein-1; ASK1, apoptosis signal-regulating kinase 1; COL1A1, collagen type 1 α1; COX-2, cyclo-oxygenase 2; CYP2E1, cytochrome P450 2E1; GAPDH, glyceraldehyde-3-phosphate dehydrogenase; GPx, glutathione peroxidase; 4-HNE, 4-hydroxynonenal; ICAM-1, intercellular adhesion molecule-1; IκB, inhibitor of NF-κB; IL-1β, interleukin-1β; iNOS, inducible nitric oxide synthase; MAPK, mitogen-activated protein kinase; MCP-1, monocyte chemotactic protein-1; MDA, malondialdehyde; MPT, mitochondrial permeability transition; MyD88, myeloid differentiation factor 88; NF-κB, nuclear factor-κB; NOX, nonphagocytic oxidase; PI3K, phosphatidylinositol-3 kinase; PPC, polyenephosphatidylcholine; SDS-PAGE, sodium dodecyl sulfate-polyacrylamide gel electrophoresis; αSMA, α smooth muscle actin; SD, standard deviation; SOD, superoxide dismutase; TNF-α, tumor necrosis factor-α; TUNEL, terminal deoxynucleotidyl transferase-mediated deoxyuridine triphosphate nick-end labeling.

0168-8278/$36.00 © 2009 European Association for the Study of the Liver. Published by Elsevier B.V. All rights reserved.
doi:10.1016/j.jhep.2009.01.025

1. Introduction

Chronic alcohol consumption can cause a wide spectrum of liver abnormalities that ranges from simple steatosis to hepatitis, cirrhosis, and hepatocellular carcinoma. It has been reported that alcoholic liver disease (ALD) remains the most common cause of liver cirrhosis in Western countries [1]. Since the appearance of hepatitis is a predictor of progression to cirrhosis and liver cancer, appropriate therapeutic intervention at this point is important in treating ALD.

Numerous data on the pathogenesis of ALD have been obtained from animal studies [1–3]. Chronic alcohol consumption induces hepatic oxidative stress due to increased generation of reactive oxygen species (ROS) and/or reduced anti-oxidant capacity. Oxidative stress causes further lipid peroxidation, which can directly damage the membranes of cells and organelles and lead to release of reactive aldehydes with potent pro-inflammatory and pro-fibrotic properties. Chronic alcohol intake also increases gut-derived lipopolysaccaride (LPS) concentration in portal blood, which binds to Toll-like receptor 4 (TLR4)/CD14 complexes and activates nuclear factor-kappa B (NF-κB), triggering pro-inflammatory responses such as induction of tumor necrosis factor-α (TNF-α) and interleukin-1β (IL-1β). Furthermore, ethanol is singularly so toxic that it can induce hepatocyte apoptosis by itself. These mechanisms are all presumed to contribute to human ALD to varying degrees.

Peroxisome proliferator-activated receptors (PPARs) are ligand-activated nuclear receptors belonging to the steroid/thyroid hormone receptor superfamily. Three isoforms of PPARs exist, designated as PPARα, PPARβ/δ, and PPARγ. Of these, PPARα is associated with the control of fatty acid transport and metabolism primarily in the liver [4]. A close relationship between PPARα and the development of ALD is believed to exist since chronic alcohol consumption decreases hepatic PPARα expression and suppresses the transcriptional activity of PPARα-regulated genes [5,6]. We previously reported that PPARα-null (*Ppara*$^{-/-}$) mice fed a 4% ethanol-containing Lieber-DeCarli diet for 6 months exhibited hepatomegaly, macrovesicular steatosis, hepatocyte apoptosis, mitochondrial swelling, hepatitis, and hepatic fibrosis, all of which resembled the clinical and pathological features of patients with ALD [7]. These abnormalities appeared with very high reproducibility and stressful surgical procedures to increase alcohol levels, such as gastric tube insertion, were not required. Therefore, *Ppara*$^{-/-}$ mice are regarded as a useful animal model to investigate the pathogenesis of human ALD.

Essential phospholipids are highly-purified phosphatidylcholine fractions containing linoleic acid and other unsaturated fatty acids. Polyenephosphatidylcholine (PPC), a major active ingredient in essential phospholipids, has a high bioavailability and affinity for cellular and subcellular membranes and maintains membrane fluidity and function. Several experiments have demonstrated the hepatoprotective effects of PPC [8–10]. However, the precise molecular mechanism of PPC action against ethanol toxicity has not been fully elucidated *in vivo*, which prompted us to evaluate the effects of PPC on ALD in greater detail using *Ppara*$^{-/-}$ mice.

2. Methods

2.1. Mice and treatment

Generation of *Ppara*$^{-/-}$ mice on a Sv/129 genetic background was described previously [11]. The mice were housed in an environment controlled for temperature, humidity, and light (25 °C, 12-h light/dark cycle) and maintained with standard laboratory chow and tap water *ad libitum* until 12 weeks of age. Male 12-week-old Sv/129 wild-type or *Ppara*$^{-/-}$ mice ($n = 24$ in each genotype) weighing 31–35 g were selected, randomly divided into 4 groups, and pair-fed the following diet for 6 months: (1) control Lieber-DeCarli liquid diet ($n = 6$); (2) control liquid diet with PPC (30 mg/kg/day) ($n = 6$); (3) 4% ethanol-containing Lieber-DeCarli liquid diet ($n = 6$); and (4) 4% ethanol-containing liquid diet with PPC (30 mg/kg/day) ($n = 6$). The ethanol-containing diet consisted of 19.4% (per weight basis) protein as casein, 51.0% carbohydrate as sucrose, 13.2% olive oil, 3.6% corn oil, 4.5% cellulose, 2.9% mineral mix, 1.1% vitamin mix, 0.3% choline bitartrate, and 4% ethanol (Oriental Yeast Co., Ltd, Tokyo, Japan). The control diet was replaced ethanol with isocaloric sucrose. PPC was provided from Alfresa (Osaka, Japan), and mixed in with the diet. Ethanol concentrations were raised gradually from 2% to 4% over the first month and maintained at 4% for the remainder of the administration period. Dietary intake was recorded every day and body weight was measured once a week. Six months after commencing treatment, all mice were sacrificed under anesthesia. After obtaining portal blood, livers were removed and weighed. All animal experiments were conducted in accordance with animal study protocols outlined in the "Guide for the Care and Use of Laboratory Animals" prepared by the National Academy of Sciences and approved by Shinshu University School of Medicine.

2.2. Measurement of plasma ethanol concentrations

To ascertain the amount of ethanol intake, blood was obtained from a tail vein at the same time (AM 10:00) of the first day of each month, and plasma ethanol concentration was determined using the vial equilibration method, as described elsewhere [7].

2.3. Preparation of nuclear and cytosolic fractions

Nuclear and cytosolic fractions were prepared as described previously [12].

2.4. Immunoblot analysis

Protein concentrations were measured colorimetrically with a BCA™ Protein Assay kit (Pierce, Rockford, IL, USA). For analysis of NF-κB, nuclear fractions (100 μg of protein) were subjected to 10% SDS–polyacrylamide gel electrophoresis (SDS–PAGE). For analysis of other proteins, whole lysate or cytosolic fractions (50–100 μg of protein) were subjected to 8–10% SDS–PAGE [12–15]. The samples were obtained from all *Ppara*$^{-/-}$ mice ($n = 6$ in each group). In each electrophoresis assay, samples from three different mice in the same group were loaded. After electrophoresis, the proteins were transferred

to nitrocellulose membranes and incubated with the primary antibody followed by alkaline phosphatase-conjugated goat anti-rabbit IgG. Antibodies raised against cytochrome P450 2E1 (CYP2E1), acyl-coenzyme A oxidase (AOX), and catalase were described previously [4,7]. Antibodies against other proteins were purchased commercially (BD Transduction Laboratories, San Diego, CA, USA for cytochrome *c* antibody, Cell Signaling Technology, Beverly, MA, USA for phosphorylated kinases, and Santa Cruz Biotechnology, Santa Cruz, CA, USA for others). The antibody against protein kinase C (PKC) recognized all PKC isoforms. Actin or histone H1 bands were used as loading controls. Band intensity was measured densitometrically, normalized to that of actin or histone H1, and expressed as fold change relative to that of *Ppara*$^{-/-}$ mice fed a control Lieber-DeCarli liquid diet without addition of PPC. For confirmation of data reproducibility, immunoblot analysis using the same samples was done twice. Similar immunoblot analysis was also performed with the remaining three samples from each group. Overall, four independent assays were carried out for each target molecule and the data of 12 band intensities were obtained for each group and subjected to statistical analysis.

2.5. Analysis of mRNA

Total liver RNA was extracted from all *Ppara*$^{-/-}$ mice ($n = 6$ in each group) using an RNeasy Mini Kit (Qiagen, Tokyo, Japan), and cDNA was generated by SuperScript II reverse transcriptase (Gibco BRL, Paisley, Scotland) [16]. Quantitative RT-PCR was performed using a SYBR green PCR kit and ABI Prism 7700 Sequence Detection System (Applied Biosystems, Foster City, CA, USA). The primer pairs used are shown in Supplementary Table 1. Measured mRNA levels were normalized to glyceraldehyde-3-phosphate dehydrogenase (GAPDH) mRNA levels, and expressed as fold change relative to those of *Ppara*$^{-/-}$ mice fed a control Lieber-DeCarli liquid diet without addition of PPC.

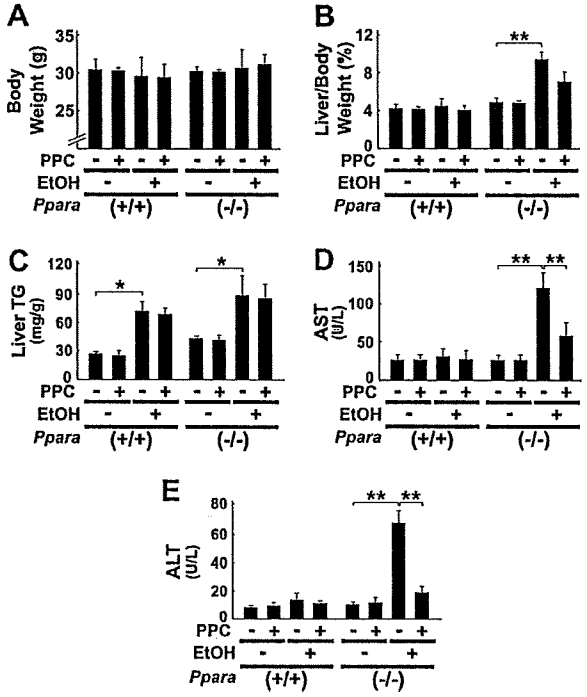

Fig. 1. General effects of PPC in 4% ethanol-treated mice. Male wild-type (+/+) and *Ppara*-null (−/−) mice were pair-fed a control- or 4% ethanol (EtOH)-containing liquid diet with or without PPC (30 mg/kg/day) for six months. The body weights (A), the degrees of hepatomegaly and liver TG accumulation (B and C), and serum levels of AST and ALT (D and E) are shown. Results are expressed as mean ± SD (n = 6/group). $^{**}P < 0.01$; $^{*}P < 0.05$.

2.6. Histological evaluation

Small blocks of liver tissue from each mouse were fixed in 4% paraformaldehyde in phosphate-buffered saline and embedded in paraffin. Sections (4 μm thick) were stained with hematoxylin and eosin or Azan-Mallory method. At least three discontinuous liver sections were evaluated in each mouse. Histological findings were scored by an independent pathologist in a blinded fashion according to the following criteria: (1) grade of steatosis: 0, none; 1, mild (5–33% of parenchymal involvement by steatosis); 2, moderate (33–66%); 3, severe (>66%); (2) activity of inflammation: 0, none; 1, mild; 2, moderate; 3, severe; and (3) stage of fibrosis: 0, none; 1, mild perisinusoidal fibrosis mainly in zone 3; 2, moderate perisinusoidal fibrosis in zone 3; 3, perisinusoidal or portal/periportal fibrosis; 4, perisinusoidal and portal/periportal fibrosis. The overall inflammation score was expressed as the sum of portal (0–3) and lobular (0–3) inflammation scores and ranged from 0 to 6. The number of necrotic foci was counted in 20 randomly selected 200× microscopic fields per section and expressed as number per square millimeter [17]. The number of neutrophils infiltrating into liver lobuli was

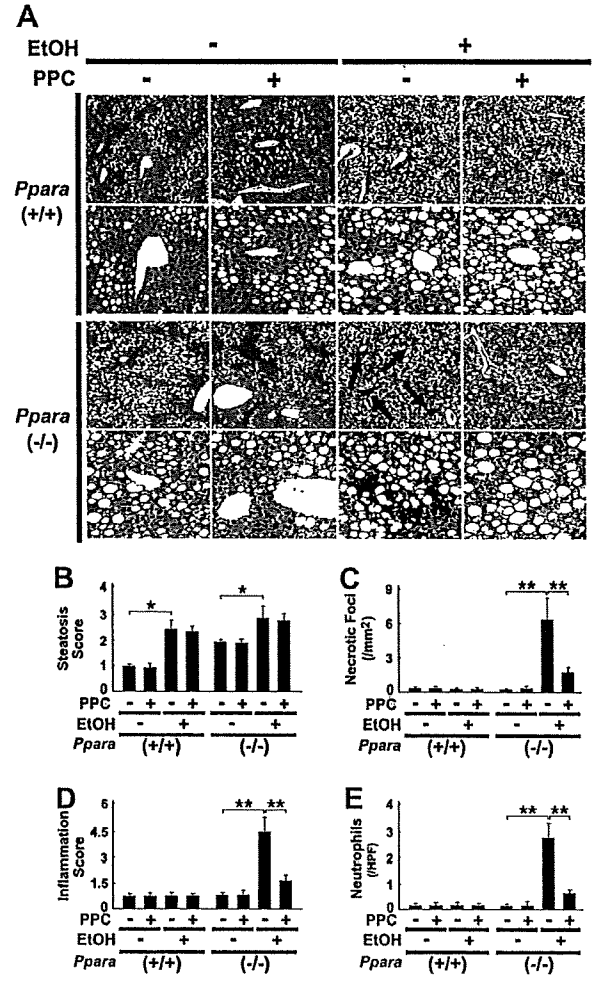

Fig. 2. Effects of PPC on liver histology in 4% ethanol-treated mice. (A) Light micrographs of liver stained by hematoxylin and eosin method. Upper and lower rows in each genotype show a magnification of 100× and 400×, respectively. Macrovesicular steatosis was found in all groups, but intralobular and periportal inflammations (arrows) were evident only in ethanol (EtOH)-fed *Ppara*-null (−/−) mice without PPC treatment. (B–E) Semiquantitative evaluation of histological findings. These assays were carried out as described in Section 2. Results are expressed as mean ± SD (n = 6/group). $^{**}P < 0.01$; $^{*}P < 0.05$.

counted in 20 randomly selected 400× microscopic fields per section and expressed as number per high-power field. To assess hepatocyte apoptosis, the terminal deoxynucleotidyl transferase-mediated deoxyuridine triphosphate nick-end labeling (TUNEL) assay was performed using MEBSTAIN Apoptosis Kit II (Medical & Biological Laboratories, Nagoya, Japan). Two-hundred hepatocytes were examined in each section, and the number of TUNEL-positive hepatocytes was expressed as a percentage [12].

2.7. Other methods

Assays for enzymatic activity were carried out as described previously [7,18]. Plasma concentrations of aspartate and alanine aminotransferase (AST and ALT) were examined using a GOT and GPT-test kit (Wako), respectively. Plasma LPS level was measured by means of an endotoxin single-test kit (Wako). Total hepatic lipids were extracted according to a method by Folch et al. [19], and levels of triglycerides (TG) and lipid peroxides [malondialdehyde (MDA) and 4-hydroxynonenal (4-HNE)] were measured with a Triglyceride *E*-test (Wako) and LPO-586 kit (OXIS International, Portland, OR, USA), respectively.

2.8. Statistical analysis

Statistical analysis was performed using the two-tailed Student's *t*-test. Quantitative data were expressed as mean ± standard deviation (SD). A probability value of less than 0.05 was considered to be statistically significant.

3. Results

3.1. General effect of PPC in 4% ethanol-fed mice

All mice survived treatment and the body weights of mice did not differ in each genotype (Fig. 1A). Although liver TG contents were increased in wild-type and *Ppara*$^{-/-}$ mice fed a 4% ethanol-containing diet, hepatomegaly and significant elevation of serum AST and ALT levels were observed only in ethanol-treated *Ppara*$^{-/-}$ mice (Fig. 1B, D, and E), which were consistent with the previous report [7]. In histological examinations, focal necrosis of hepatocytes and infiltration of inflammatory cells, mainly neutrophils, were detected only in *Ppara*$^{-/-}$ mice fed the liquid diet containing ethanol, but ballooned hepatocytes or Mallory's hyaline were not found (Fig. 2A, C–E). Moderate-to-severe macrovesicular steatosis was seen in all groups (Fig. 2A and B). PPC did not have any effects on hepatomegaly or hepatic TG accumulation (Fig. 1B and C), but significantly improved serum AST and ALT levels (Fig. 1D and E) and activity of hepatitis (Fig. 2A, C–E) in ethanol-fed *Ppara*$^{-/-}$ mice. These results demonstrate that PPC could alleviate ethanol-induced hepatocyte damage and hepatitis occurred specifically in *Ppara*$^{-/-}$ mice.

3.2. Effect of PPC on ethanol metabolism

To explore the mechanism of PPC action on ALD in *Ppara*$^{-/-}$ mice, we first examined the changes in ethanol-metabolizing enzymes in the liver. Plasma ethanol concentrations were similar between *Ppara*$^{-/-}$ mice fed ethanol-containing diets with or without PPC (36 ± 12 vs. 34 ± 14 mM at one month; 45 ± 12 vs. 44 ± 10 mM at 2 months; and 46 ± 6 vs.

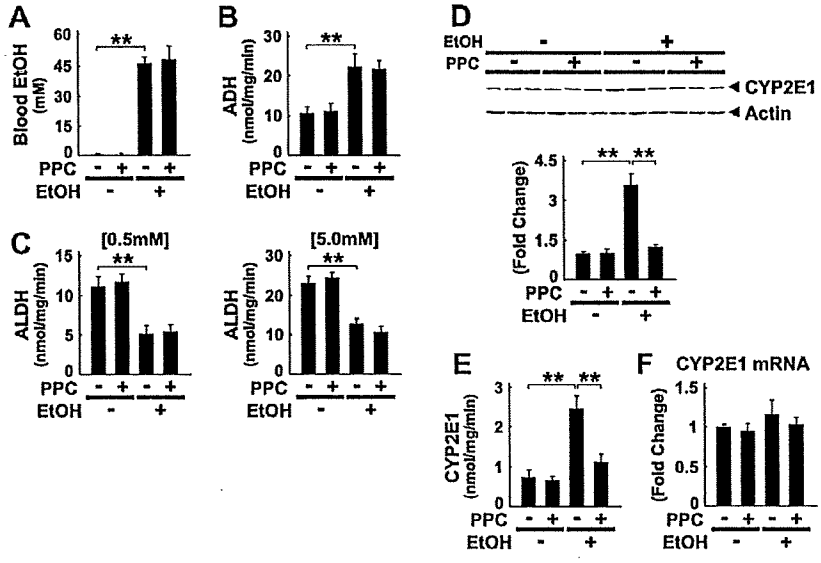

Fig. 3. Analyses of factors associated with ethanol metabolism in *Ppara*$^{-/-}$ mice. (A–C) Blood concentrations of ethanol (EtOH, A) and hepatic activities of ADH (B) and ALDH at low (0.5 mM) and high (5.0 mM) acetaldehyde concentrations (C). Results are expressed as mean ± SD (n = 6/group). $^{**}P < 0.01$. (D) Immunoblot analysis of CYP2E1. Whole liver lysates (50 μg of protein) obtained from three different mice in each group were loaded. Actin was used as the loading control. The bands shown are representative of four independent experiments. Band intensity was quantified densitometrically, normalized to that of actin, and subsequently normalized to that in control *Ppara*$^{-/-}$ mice. Results are expressed as mean ± SD (n = 6/group). $^{**}P < 0.01$. (E) Hepatic activities of CYP2E1. Results are expressed as mean ± SD (n = 6/group). $^{**}P < 0.01$. (F) Levels of CYP2E1 mRNA. CYP2E1 mRNA levels were normalized to those of GAPDH and subsequently normalized to those in control *Ppara*$^{-/-}$ mice. Results are expressed as mean ± SD (n = 6/group).

47 ± 14 mM at 4 months), as well as those at the endpoint (Fig. 3A). Although PPC did not change the levels of alcohol dehydrogenase (ADH) or aldehyde dehydrogenase (ALDH) activity (Fig. 3B and C), it normalized increases in the expression and activity of CYP2E1 (Fig. 3D and E). Quantitative RT-PCR analysis revealed that the changes in CYP2E1 expression were due to a post-transcriptional mechanism (Fig. 3F).

3.3. Effect of PPC on hepatic oxidative stress

To test whether PPC modified the ROS production caused by ethanol intake, the hepatic content of lipid peroxides MDA and 4-HNE were determined. As expected, PPC halted increases in these byproducts (Fig. 4A and B). PPC diminished the induction of ROS-generating enzymes AOX and NADPH oxidase NOX-2 (Fig. 4C), and the same was true for changes in their mRNA levels (Fig. 4D). Furthermore, PPC alleviated the increases in NOX-4 (Fig. 4C). On the other hand, PPC did not influence either the expression of ROS-eliminating enzymes, such as Cu, Zn-superoxide dismutase (SOD), Mn-SOD, catalase, and glutathione peroxidase (GPx), or the activities of SOD and GPx (Fig. 4C, E, and F). Additionally, PPC did not have any impact on the activity of glutathione S-transferase or glutathione content in the liver

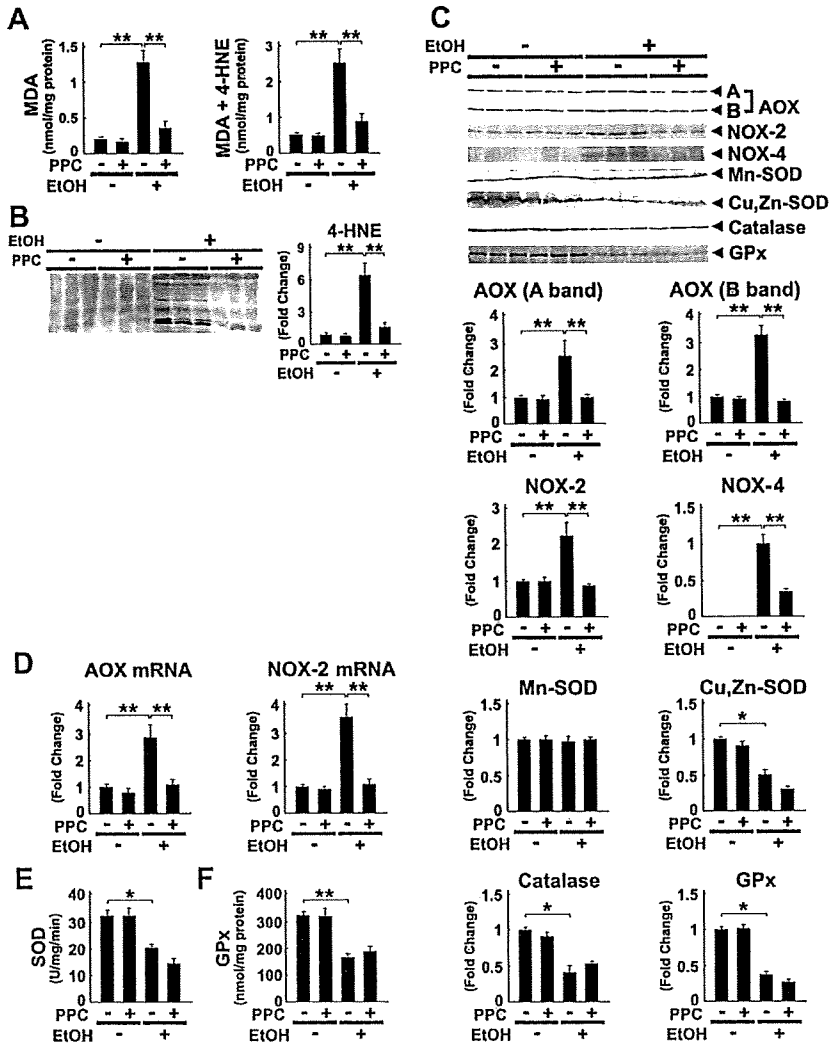

Fig. 4. Ethanol-induced increases in oxidative stress were inhibited by PPC treatment in *Ppara*$^{-/-}$ mice. (A) Hepatic contents of lipid peroxides. Results are expressed as mean ± SD (n = 6/group). $^{**}P < 0.01$. (B and C) Immunoblot analysis of 4-HNE and ROS-generating and ROS-eliminating enzymes. The same samples used in Fig. 3D (whole liver lysate, 50 μg of protein) were adopted. The bands shown are representative of four independent experiments. Band intensity was quantified densitometrically, normalized to that of actin, and subsequently normalized to that in control *Ppara*$^{-/-}$ mice. Results are expressed as mean ± SD (n = 6/group). A and B bands of AOX, full-length and truncated AOX, respectively; $^{**}P < 0.01$; $^{*}P < 0.05$. (D) Levels of AOX and NOX-2 mRNA. The mRNA levels were normalized to those of GAPDH and subsequently normalized to those in control *Ppara*$^{-/-}$ mice. Results are expressed as mean ± SD (n = 6/group). $^{**}P < 0.01$. (E and F) Activities of SOD and GPx in the liver. $^{**}P < 0.01$; $^{*}P < 0.05$.

(data not shown). Overall, it appears that PPC contributed to decreases in ethanol-derived oxidative stress by inhibiting the overexpression of ROS-generating enzymes, but not by reinforcing anti-oxidant defense capacity.

3.4. Effect of PPC on kinase phosphorylation

Since ROS can serve as a second messenger in signal transduction by activating various stress kinases, the degree of phosphorylation of these enzymes was examined. Continuous ethanol administration increased the phosphorylated forms of apoptosis signal-regulating kinase 1 (ASK1), p38 mitogen-activated protein kinase (p38 MAPK), PKC, and phosphatidylinositol-3 kinase (PI3K) (Fig. 5). However, PPC significantly suppressed the increases in each of these proteins (Fig. 5).

3.5. Effect of PPC on the NF-κB-mediated signaling pathway

PPC normalized the increases in NF-κB subunits p65 and p50 in hepatocyte nuclei of ethanol-fed mice (Fig. 6A). To determine whether the activation of NF-κB was the result of degradation of IκB-α, an inhibitor of NF-κB, the expression of IκB-α and its phosphorylated form (p-IκB-α) was assessed by immunoblot analysis. Ethanol caused marked decreases in IκB-α and increases in p-IκB-α, but PPC corrected these changes (Fig. 6B), thus ameliorating the ethanol-enhanced increases in mRNA levels of NF-κB-regulated genes, including TNF-α, IL-1β, cyclo-oxygenase 2 (COX-2), inducible nitric oxide synthase (iNOS), intercellular adhesion molecule 1 (ICAM-1), and monocyte chemotactic protein 1 (MCP-1) (Fig. 6C). Collectively, these results indicate that PPC significantly attenuated NF-κB activation and the resultant pro-inflammatory responses induced by persistent ethanol consumption.

3.6. Effect of PPC on the LPS-mediated signaling pathway

Since gut-derived LPS is also known to be a potent activator of NF-κB, the effect of PPC on portal LPS concentrations was examined. These concentrations were raised by the end of the treatment period in ethanol-fed mice, but were not improved by PPC (Fig. 7A). On the other hand, PPC suppressed ethanol-induced increases in mRNA levels of TLR4 and CD14 (Fig. 7B). The mRNA levels of myeloid differentiation factor 88 (MyD88), an essential adapter molecule that combines with TLR4/CD14, remained unchanged in all groups (Fig. 7B). PPC appears to prevent ethanol-induced amplification of the LPS-mediated signaling pathway.

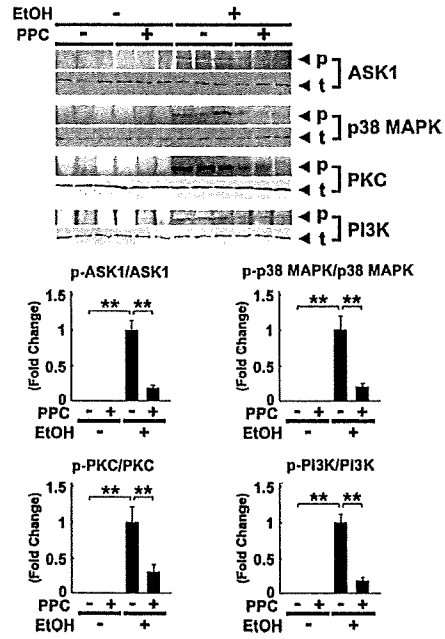

Fig. 5. Immunoblot analysis of representative stress kinases and their phosphorylated forms using *Ppara*$^{-/-}$ mouse livers. The same samples used in Fig. 3D (whole liver lysate, 100 μg of protein) were used. The bands shown are representative of four independent experiments. The band intensity of phosphorylated proteins was quantified densitometrically, normalized to that of the corresponding total protein, and subsequently normalized to that in the EtOH-fed *Ppara*$^{-/-}$ mice without PPC treatment since phosphorylated proteins could not be detected in controls. Results are expressed as mean ± SD (n = 6/group). p, phosphorylated protein; t, total protein; $^{**}P < 0.01$.

3.7. Effect of PPC on hepatocyte apoptosis

PPC significantly decreased the number of TUNEL-positive hepatocytes and caspase 3 activity in ethanol-fed mice (Fig. 8A–C). PPC also suppressed increases in Bax and truncated Bid (Fig. 8D) and blocked activation of mitochondrial permeability transition (MPT), as revealed by the absence of cytochrome *c* leakage to the cytoplasm (Fig. 8E). In contrast, PPC did not influence the expression of anti-apoptotic proteins, such as Bcl-2 and Bcl-xL (Fig. 8D).

3.8. Effect of PPC on hepatic fibrosis

Lastly, PPC inhibited perisinusoidal fibrosis in chronically ethanol-administered mice (Fig. 9A and B). This finding was corroborated by quantification of collagen type 1 α1 (COL1A1) mRNA levels (Fig. 9C). PPC also inhibited ethanol-induced increases in the expression of pro-fibrotic cytokines transforming growth factor-β1 (TGF-β1) and TGF-α, as well as that of α-smooth muscle actin (αSMA), an indicator of hepatic stellate cell activa-

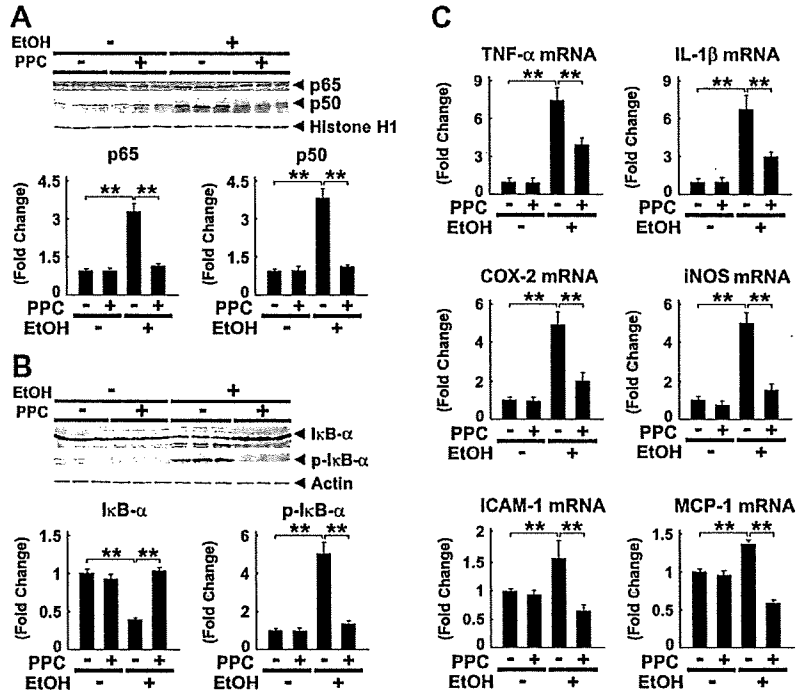

Fig. 6. Ethanol-induced NF-κB activation and increases in pro-inflammatory responses were blocked by PPC treatment in *Ppara*$^{-/-}$ mice. (A) Immunoblot analysis of NF-κB subunits p65 and p50. Nuclear fractions obtained from three different mice in each group (100 μg of protein) were loaded. Histone H1 was used as the loading control. The bands are representative of four independent experiments. Band intensity was quantified densitometrically, normalized to that of histone H1, and subsequently normalized to that in the control *Ppara*$^{-/-}$ mice. Results are expressed as mean ± SD (n = 6/group). $^{**}P < 0.01$. (B) Immunoblot analysis of IκB-α and its phosphorylated form. Cytosolic fractions obtained from three different mice in each group (100 μg of protein) were loaded. The bands shown are representative of four independent experiments. Band intensity was quantified densitometrically, normalized to that of actin, and subsequently normalized to that in the control *Ppara*$^{-/-}$ mice. Results are expressed as mean ± SD (n = 6/group). $^{**}P < 0.01$. (C) Levels of mRNA of NF-κB-regulated genes. The mRNA levels were normalized to those of GAPDH and subsequently normalized to those in control *Ppara*$^{-/-}$ mice. Results are expressed as mean ± SD (n = 6/group). $^{**}P < 0.01$.

tion (Fig. 9D). Taken together, these results demonstrate that PPC exhibited an anti-fibrotic effect against ALD.

4. Discussion

The present study characterized the diverse hepatoprotective effects of PPC on ALD in *Ppara*$^{-/-}$ mice. Namely, we identified a novel and unique mechanism involving attenuation of hepatic ROS generation through down-regulation of CYP2E1, AOX, NOX-2, and NOX-4. Such action differs from that of well-known anti-oxidants tocopherol and S-adenosyl methionine, which restores glutathione content [1,20]. The peculiar properties of PPC to inhibit ROS production are considered to be essential in the down-regulation of several signal transduction pathways activated by ethanol, i.e., ROS-PKC-PI3K-NF-κB, ROS-ASK1-p38 MAPK, ROS-TLR4/CD14, and ROS-Bax/tBid-MPT activation. These findings enabled us to propose detailed mechanisms of the anti-oxidant effect of PPC.

Chronic ethanol exposure leads to a metabolic shift from ADH to CYP2E1 in the liver, which is largely responsible for the overproduction of ROS [1–3]. Our results demonstrated that ethanol significantly increased hepatic CYP2E1 expression at the post-transcriptional level in mice. Chronic ethanol consumption is also known to cause protein accumulation in hepatocytes because of decreased protein-catabolizing ability in proteasomes [21]. Considering that there was an inverse correlation between proteasomal activity and hepatic amounts of lipid peroxides [22], as well as the fact that decreases in proteasomal activity were not detected in ethanol-fed CYP2E1-knockout mice [23], we can speculate that CYP2E1-derived oxidative stress plays an essential role in proteasomal dysfunction in ALD. Since CYP2E1 itself is also degraded by proteasomes [24], ethanol-induced oxidative stress may down-regulate the proteasomal degradation pathway and increase CYP2E1 expression, thus further overproducing ROS. The finding that PPC can discontinue this vicious cycle is consistent with recent evidence that choline facilitates proteasomal degradation of phosphoethanolamine methyltransferase [25]. However, it remains to be elucidated how either PPC or choline improves proteasomal activity.

A novel and unexpected result in this study was that AOX mRNA levels, encoding a rate-limiting enzyme in

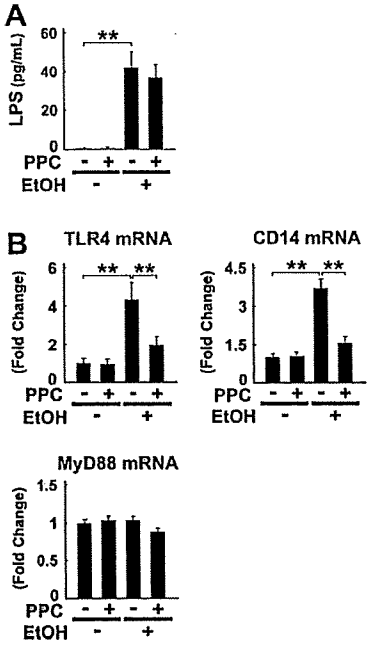

Fig. 7. Ethanol-induced increases in TLR4/CD14 were suppressed by PPC treatment in *Ppara*$^{-/-}$ mice. (A) Portal LPS concentrations. $^{**}P < 0.01$. (B) Levels of mRNA of genes associated with the LPS-mediated signaling pathway. Results are expressed as mean ± SD ($n = 6$/group). $^{**}P < 0.01$.

the peroxisomal β-oxidation pathway, were increased in ethanol-fed *Ppara*$^{-/-}$ mice but normalized by PPC. The same alterations were confirmed in the expression of other peroxisomal enzymes, such as peroxisomal hydratase and thiolase (data not shown). Since these enzymes are known to be induced by PPARα activation [4], it is plausible that PPARα-independent mechanisms also exist to induce such enzymes [26]. Indeed, Latruffe et al. previously showed that PKC activation might be associated with increases in mRNA levels of peroxisomal β-oxidation enzymes [27]. PKC was markedly phosphorylated in ethanol-treated *Ppara*$^{-/-}$ mice, implying that ethanol-derived ROS may have activated PKC resulting in induction of AOX in a PPARα-independent manner, thus generating further ROS. Therefore, we believe that PPC reduces CYP2E1-derived ROS, prevents activation of PKC, and possibly inhibits overexpression of AOX.

The observation that PPC inhibits NF-κB activation is consistent with the previous result that dilinoleoylphosphatidylcholine decreases acetaldehyde-induced NF-κB activation and TNF-α generation in isolated Kupffer cells [9]. NF-κB activated by ROS and acetaldehyde induces the enhancement of NOX-2 expression, whose gene contains an NF-κB response element in its promoter region [28]. Furthermore,

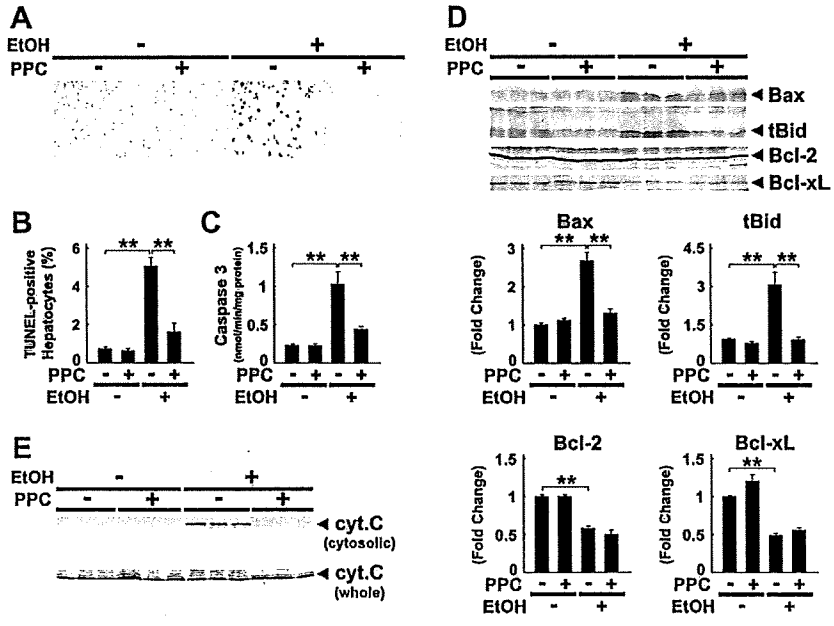

Fig. 8. Ethanol-induced hepatocyte apoptosis was prevented by PPC treatment in *Ppara*$^{-/-}$ mice. (A and B) Apoptotic hepatocytes as determined by TUNEL staining. Two-hundred hepatocytes were examined for each section, and the number of TUNEL-positive hepatocytes was expressed as a percentage. Results are expressed as mean ± SD ($n = 6$/group). $^{**}P < 0.01$. (C) Activity of caspase 3. $^{**}P < 0.01$. (D) Immunoblot analysis of apoptosis-related proteins. The same samples in Fig. 3D (whole liver lysate, 50 μg of protein) were used. The bands shown are representative of four independent experiments. Band intensity was quantified densitometrically, normalized to that of actin, and subsequently normalized to that in control *Ppara*$^{-/-}$ mice. Results are expressed as mean ± SD ($n = 6$/group). tBid, truncated Bid; $^{**}P < 0.01$. (E) Immunoblot analysis of cytochrome *c* (cyt. *c*). The same samples used in Fig. 3D (whole liver lysate, 50 μg of protein) and Fig. 6B (cytosolic fraction, 100 μg of protein) were adopted. Results are representative of four independent experiments.

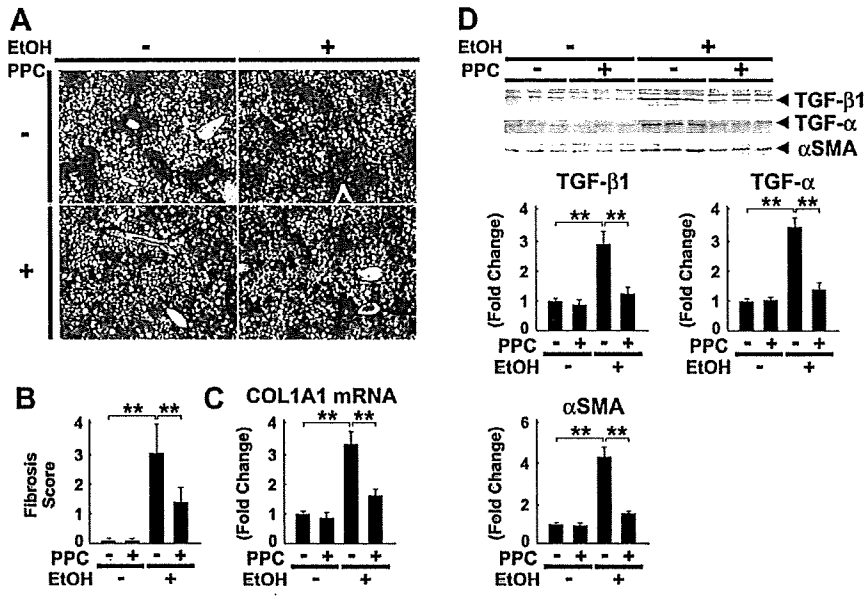

Fig. 9. Ethanol-induced hepatic fibrosis was alleviated by PPC treatment in *Ppara*$^{-/-}$ mice. (A and B) Liver sections were subjected to Azan-Mallory staining and the degree of fibrosis was assessed according to the grading system described in Section 2. Results are expressed as mean ± SD (n = 6/group). $^{**}P < 0.01$. (C) Levels of COL1A1 mRNA. COL1A1 mRNA levels were normalized to those of GAPDH and subsequently normalized to those in control *Ppara*$^{-/-}$ mice. $^{**}P < 0.01$. (D) Immunoblot analysis of molecules contributing to fibrogenesis. The same samples in Fig. 3D (whole liver lysate, 50 μg of protein) were used. The bands shown are representative of four independent experiments. Band intensity was quantified densitometrically, normalized to that of actin, and subsequently normalized to that in control *Ppara*$^{-/-}$ mice. Results are expressed as mean ± SD (n = 6/group). $^{**}P < 0.01$.

NF-κB activation can induce the expression of iNOS, another major source of ROS. Therefore, activated NF-κB strongly amplifies generation of ROS, which further activates oxidative stress-responsive transcriptional factors, including NF-κB itself and activator protein 1 (AP-1). PPC is presumed to block this harmful spiral.

PPC did not decrease portal concentrations of LPS, suggesting only a minor contribution to gut flora and integrity of the intestinal mucosal barrier. On the other hand, we found for the first time that PPC significantly suppressed increases in TLR4/CD14 expression, which probably prevented amplification of LPS-mediated signals by ethanol. The transcriptional activity of TLR4/CD14 is enhanced by NF-κB and/or AP-1, whose binding sites are found in the promoter regions of both genes [29,30]. Moreover, induction of the TLR4 gene can also result from post-transcriptional stabilization of mRNA by activation of p38 MAPK [29]. Therefore, the suppressive effect of PPC on hepatic TLR4/CD14 levels seems to occur through the diminishment of oxidative stress.

COL1A1 and COL1A2 genes, encoding collagen type 1 α1 and α2 chains, respectively, are highly sensitive to ROS. The COL1A2 promoter possesses TGF-β1-, TNF-α-, and NF-κB-binding sites, and its transcription is reported to be activated through a lipid peroxidation-PKC-PI3K-NF-κB-driven mechanism [31]. Thus, PPC is suspected to inhibit collagen synthesis by reducing ROS, down-regulating TGF-β1, and inactivating the PKC- PI3K-NF-κB-mediated pathway.

It is quite noteworthy that PPC markedly corrected the increases in hepatic NOX-4 expression caused by chronic ethanol consumption. Because of trace amounts of NOX-4 in normal livers, little information has been available regarding the contribution of this NOX isoform to various liver diseases. However, a recent study demonstrated a central role in the process of TGF-β-induced hepatocyte apoptosis [32]. Furthermore, overexpression of NOX-4 was detected in the livers of human ALD [33]. Thus, down-regulation of NOX-4 by PPC is considered to be one of the molecular mechanisms of its anti-oxidant and anti-apoptotic properties.

It has been reported that the expression of molecules contributing to fibrogenesis (TGF-β1, COL1A1, and αSMA) and inflammation (MCP-1) was significantly up-regulated in human livers with alcoholic hepatitis, and was strongly correlated with disease severity [33]. Since these increases were also found in 4% ethanol-fed *Ppara*$^{-/-}$ mice, the mechanism documented in the present study might, at least in part, apply to human ALD. Although there was a trend towards improvement of serum ALT levels in PPC-treated groups in a long-term trial in patients with alcoholic cirrhosis, the full spectrum of PPC benefits have not been evaluated appropriately because of the dramatic reduction in alcohol consumption in the treated and placebo groups [34]. Thus, PPC might deserve re-examination for its efficacy

in patients with alcoholic hepatitis, especially in non-cirrhotic ones.

In conclusion, we were able to uncover the precise mechanism of PPC in the amelioration of ethanol-induced oxidative stress, which was distinct from other anti-oxidants. These data raise the possibility that PPC might be beneficial in chronic liver diseases associated with increased oxidative stress, including ALD, nonalcoholic steatohepatitis, and chronic hepatitis C [35,36]. Further studies are needed to confirm the efficacy of PPC against these diseases.

Acknowledgement

We thank Trevor Ralph for his editorial assistance.

Appendix A. Supplementary data

Supplementary data associated with this article can be found, in the online version, at doi:10.1016/j.jhep.2009.01.025.

References

[1] Tilg H, Day CP. Management strategies in alcoholic liver disease. Nat Clin Pract Gastroenterol Hepatol 2007;4:24–34.
[2] Lieber CS. Alcoholic fatty liver: its pathogenesis and mechanism of progression to inflammation and fibrosis. Alcohol 2004;34:9–19.
[3] Seitz HK, Lieber CS, Stickel F, Salaspuro M, Schlemmer HP, Horie Y. Alcoholic liver disease: from pathophysiology to therapy. Alcohol Clin Exp Res 2005;29:1276–1281.
[4] Aoyama T, Peters JM, Iritani N, Nakajima T, Furihata K, Hashimoto T, et al. Altered constitutive expression of fatty acid-metabolizing enzymes in mice lacking the peroxisome proliferator-activated receptor α (PPARα). J Biol Chem 1998;273:5678–5684.
[5] Galli A, Pinaire J, Fischer M, Dorris R, Crabb DW. The transcriptional and DNA binding activity of peroxisome proliferator-activated receptor α is inhibited by ethanol metabolism. A novel mechanism for the development of ethanol-induced fatty liver. J Biol Chem 2001;276:68–75.
[6] Fischer M, You M, Matsumoto M, Crabb DW. Peroxisome proliferator-activated receptor α (PPAR α) agonist treatment reverses PPAR α dysfunction and abnormalities in hepatic lipid metabolism in ethanol-fed mice. J Biol Chem 2003;278:27997–28004.
[7] Nakajima T, Kamijo Y, Tanaka N, Sugiyama E, Tanaka E, Kiyosawa K, et al. Peroxisome proliferator-activated receptor α protects against alcohol-induced liver damage. Hepatology 2004;40:972–980.
[8] Lieber CS, Robins SJ, Li J, DeCarli LM, Mak KM, Fasulo JM, et al. Phosphatidylcholine protects against fibrosis and cirrhosis in the baboon. Gastroenterology 1994;106:152–159.
[9] Cao Q, Mak KM, Lieber CS. Dilinoleoylphosphatidylcholine decreases acetaldehyde-induced TNF-α generation in Kupffer cells of ethanol-fed rats. Biochem Biophys Res Commun 2002;299:459–464.
[10] Cao Q, Mak KM, Lieber CS. DLPC and SAMe combined prevent leptin-stimulated TIMP-1 production in LX-2 human hepatic stellate cells by inhibiting H_2O_2-mediated signal transduction. Liver Int 2006;26:221–231.
[11] Lee SS, Pineau T, Drago J, Lee EJ, Owens JW, Kroetz DL, et al. Targeted disruption of the α isoform of the peroxisome proliferator-activated receptor gene in mice results in abolishment of the pleiotropic effects of peroxisome proliferators. Mol Cell Biol 1995;15:3012–3022.
[12] Tanaka N, Moriya K, Kiyosawa K, Koike K, Aoyama T. Hepatitis C virus core protein induces spontaneous and persistent activation of peroxisome proliferator-activated receptor α in transgenic mice: implications for HCV-associated hepatocarcinogenesis. Int J Cancer 2008;122:124–131.
[13] Aoyama T, Uchida Y, Kelley RI, Marble M, Hofman K, Tonsgard JH, et al. A novel disease with deficiency of mitochondrial very-long-chain acyl-CoA dehydrogenase. Biochem Biophys Res Commun 1993;191:1369–1372.
[14] Aoyama T, Souri M, Ushikubo S, Kamijo T, Yamaguchi S, Kelley RI, et al. Purification of human very-long-chain acyl-coenzyme A dehydrogenase and characterization of its deficiency in seven patients. J Clin Invest 1995;95:2465–2473.
[15] Tanaka N, Hora K, Makishima H, Kamijo Y, Kiyosawa K, Gonzalez FJ, et al. In vivo stabilization of nuclear retinoid X receptor α in the presence of peroxisome proliferator-activated receptor α. FEBS Lett 2003;543:120–124.
[16] Nakajima T, Tanaka N, Sugiyama E, Kamijo Y, Hara A, Hu R, et al. Cholesterol-lowering effect of bezafibrate is independent of peroxisome proliferator-activated receptor activation in mice. Biochem Pharmacol 2008;76:108–119.
[17] Nanji AA, Jokelainen K, Rahemtulla A, Miao L, Fogt F, Matsumoto H, et al. Activation of nuclear factor-κB and cytokine imbalance in experimental alcoholic liver disease in the rat. Hepatology 1999;30:934–943.
[18] Gong P, Cederbaum AI, Nieto N. Increased expression of cytochrome P450 2E1 induces heme oxygenase-1 through ERK MAPK pathway. J Biol Chem 2003;278:29693–29700.
[19] Folch J, Lees M, Sloane Stanley GH. A simple method for the isolation and purification of total lipides from animal tissues. J Biol Chem 1957;226:497–509.
[20] Altavilla D, Marini H, Seminara P, Squadrito G, Minutoli L, Passaniti M, et al. Protective effects of antioxidant raxofelast in alcohol-induced liver disease in mice. Pharmacology 2005;74:6–14.
[21] Donohue Jr JM, Cederbaum AI, French SW, Barve S, Gao B, Osna NA. Role of the proteasome in ethanol-induced liver pathology. Alcohol Clin Exp Res 2007;31:1446–1459.
[22] Fataccioli V, Andraud E, Gentil M, French SW, Rouach H. Effects of chronic ethanol administration on rat liver proteasome activities: relationship with oxidative stress. Hepatology 1999;29:14–20.
[23] Bardag-Gorce F, Yuan QX, Li J, French BA, Fang C, Ingelman-Sundberg M, et al. The effect of ethanol-induced cytochrome p4502E1 on the inhibition of proteasome activity by alcohol. Biochem Biophys Res Commun 2000;279:23–29.
[24] Goasduff T, Cederbaum AI. NADPH-dependent microsomal electron transfer increases degradation of CYP2E1 by the proteasome complex: role of reactive oxygen species. Arch Biochem Biophys 1999;370:258–270.
[25] Witola WH, Ben Mamoun C. Choline induces transcriptional repression and proteasomal degradation of the malarial phosphoethanolamine methyltransferase. Eukaryot Cell 2007;6:1618–1624.
[26] Zhang X, Tanaka N, Nakajima T, Kamijo Y, Gonzalez FJ, Aoyama T. Peroxisome proliferator-activated receptor α-independent peroxisome proliferation. Biochem Biophys Res Commun 2006;346:1307–1311.
[27] Latruffe N, Cherkaoui Malki M, Nicolas-Frances V, Clemencet MC, Jannin B, Berlot JP. Regulation of the peroxisomal β-

oxidation-dependent pathway by peroxisome proliferator-activated receptor α and kinases. Biochem Pharmacol 2000;60: 1027–1032.
[28] Anrather J, Racchumi G, Iadecola C. NF-κB regulates phagocytic NADPH oxidase by inducing the expression of gp91^{phox}. J Biol Chem 2006;281:5657–5667.
[29] Yan ZQ. Regulation of TLR4 expression is a tale about tail. Arterioscler Thromb Vasc Biol 2006;26:2582–2584.
[30] Wheeler MD, Thurman RG. Up-regulation of CD14 in liver caused by acute ethanol involves oxidant-dependent AP-1 pathway. J Biol Chem 2003;278:8435–8441.
[31] Nieto N. Ethanol and fish oil induce NFκB transactivation of the collagen α2 (I) promoter through lipid peroxidation-driven activation of the PKC-PI3K-Akt pathway. Hepatology 2007;45:1433–1445.
[32] Carmona-Cuenca I, Roncero C, Sancho P, Caja L, Fausto N, Fernandez M, et al. Upregulation of the NADPH oxidase NOX4 by TGF-beta in hepatocytes is required for its pro-apoptotic activity. J Hepatol 2008;49:965–976.
[33] Colmenero J, Bataller R, Sancho-Bru P, Bellot P, Miquel R, Moreno M, et al. Hepatic expression of candidate genes in patients with alcoholic hepatitis: correlation with disease severity. Gastroenterology 2007;132:687–697.
[34] Lieber CS, Weiss DG, Groszmann R, Paronetto F, Schenker S for the Veterans Affairs Cooperative Study 391 Group. Veterans Affairs Cooperative Study of polyenylphosphatidylcholine in alcoholic liver disease. Alcohol Clin Exp Res 2003;27:1765–1772.
[35] Tanaka N, Sano K, Horiuchi A, Tanaka E, Kiyosawa K, Aoyama T. Highly purified eicosapentaenoic acid treatment improves nonalcoholic steatohepatitis. J Clin Gastroenterol 2008;42:413–418.
[36] Tanaka N, Moriya K, Kiyosawa K, Koike K, Gonzalez FJ, Aoyama T. PPARα activation is essential for HCV core protein-induced hepatic steatosis and hepatocellular carcinoma in mice. J Clin Invest 2008;119:683–694.

Hepatology Research 2009; 39: 207–212 doi: 10.1111/j.1872-034X.2008.00446.x

Case Report

A case of well-differentiated cholangiolocellular carcinoma visualized with contrast-enhanced ultrasonography using Sonazoid

Satoru Joshita,[1] Tetsuya Ichijo,[1] Fumitaka Suzuki,[2] Takahide Yokoyama,[2] Yukiko Sugiyama,[3] Mana Fukushima,[4] Atsushi Kamijo,[1] Michiharu Komatsu,[1] Takeji Umemura,[1] Kaname Yoshizawa,[1] Shinichi Miyagawa[2] and Eiji Tanaka[1]

[1]*Department of Internal Medicine, Division of Gastroenterology and Hepatology,* [2]*Department of Surgery,* [3]*Department of Radiology and* [4]*Department of Laboratory Medicine, Shinshu University School of Medicine, Matsumoto, Japan*

We here report the first case of cholangiolocellular carcinoma (CoCC) visualized with contrast-enhanced ultrasonography (CEUS) using a second-generation contrast agent, Sonazoid. A 76-year-old man was admitted to our hospital for evaluation of a hepatic tumor. The tumor was described as having hyperenhancement in the early phase and persistent enhancement in the late phase by contrast-enhanced computed tomography (CT) and magnetic resonance imaging (MRI), as well as hypervascularity by angiography. CEUS assessment of the nodule showed diffuse and homogeneous enhancement in the pure arterial phase, which became progressively hypoechoic relative to the adjacent liver parenchyma during the portal vein and late phases (mixed vascular phase), and showed a contrast defect with an unclear border in the Kupffer phase. Histologically we diagnosed this hepatic tumor as CoCC. In light of the above findings and the rarity of CoCC, it is helpful to incorporate the results of several imagings, such as CT, MRI, angiography and CEUS with a second-generation contrast agent when clinically diagnosing CoCC.

INTRODUCTION

CHOLANGIOLOCELLULAR CARCINOMA (COCC) was first reported as an adenocarcinoma originating from the ductules/canals of Hering.[1] Considered to be derived from hepatic stem cell carcinoma,[2] CoCC is categorized as a subtype of cholangiocellular carcinoma (CCC) based on criteria from the World Health Organization (WHO).[3] In Japan, CoCC was classified as an independent primary liver cancer in 2008.[4] CoCC has been reported to account for approximately 1% of primary liver cancers.[1] In a Japanese study, four cases of CoCC were found in 708 (0.56%) consecutively resected cases of primary liver cancer.[5] CoCC can be clinically misdiagnosed as hepatocellular carcinoma (HCC), because many patients are infected with hepatitis C or B virus.[6] Furthermore, the features of CoCC in ultrasonography have not been fully elucidated.

Contrast-enhanced ultrasonography (CEUS) is a useful tool for the diagnosis of hepatic tumors[7], the evaluation of malignancy grade and treatment response, and CEUS-guided percutaneous local ablation therapy.[7–9] Injection of Sonazoid (perfluorobutane; Daiichi-Sankyo, Tokyo, Japan),[10] a second-generation contrast agent for ultrasonography, was approved in Japan for imaging lesions associated with hepatic cancer via ultrasound in 2007. However, due to the rarity of CoCC, few studies combining the findings of CEUS, MRI, computed tomography (CT) and angiography have been reported. As such, we here present a case of CoCC that showed interesting findings under CEUS using Sonazoid.

CASE REPORT

A 76-YEAR-OLD man was admitted to our hospital for examination of a hepatic tumor located from segment 4 to 8. He had seen a doctor regularly since the

Correspondence: Dr Satoru Joshita, Department of Internal Medicine, Division of Gastroenterology and Hepatology, Shinshu University School of Medicine, 3-1-1 Asahi, Matsumoto, 390-8621, Japan. Email: joshita@shinshu-u.ac.jp
Received 06 July 2008; revision 11 August 2008; accepted 12 August 2008.

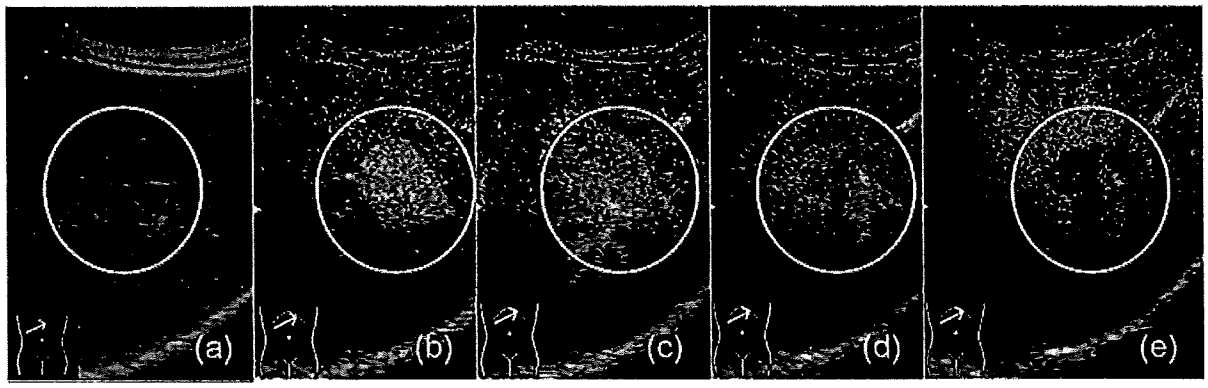

Figure 1 (a) B-mode ultrasonography showed the hepatic nodule as a heterogeneous hypoechoic lesion with an unclear border in which the middle hepatic vein was seen running through it. (b–e) Contrast enhanced ultrasonography. (b) 26 s (pure arterial phase) after contrast agent injection, the nodule showed homogeneous hyper-enhancement without invasion of vessels in and around the tumor. (c) 90 s (portal vein phase) after contrast agent administration, the tumor was isoechoic with the surrounding tissue. (d) During the late phase (180 s after injection) the nodule became hypoechoic relative to the liver parenchyma. (e) In Kupffer phase imaging (10 min after injection), it showed a contrast defect with an unclear border.

onset of chronic hepatitis C at 60 years of age. The nodular lesion was 10 mm in diameter and was first detected with B-mode ultrasonography and CT three years before admission, but had neither changed in size nor imaging characteristics since. The size of the tumor began slowly enlarging 5 months before admission.

Physical examination on admission was normal. Laboratory tests were also normal and were as follows: white blood cell count, 5340/mm;^{3} red blood cell count, 483×10^4/mm;^{3} platelet count, 145 000/mm;^{3} prothrombin time (percentage), 94.7%; albumin, 4.6 g/dL; total bilirubin, 1.1 mg/dL; aspartate aminotransferase, 19 U/L; alanine aminotransferase, 21 U/L; alkaline phosphatase, 189 U/L; and gamma-glutamyl transpeptidase, 24 U/L. Hepatitis B virus surface antigen was negative and core antibody was low strength positive. The levels of several serum tumor markers were all within the normal limits, including α-fetoprotein, 1.3 ng/mL; prothrombin induced by vitamin K absence or antagonist II, 13 mAU/mL; carcinoembryonic antigen, 2.1 ng/mL; and carbohydrate antigen 19–9, 20.7 U/mL.

The hepatic nodule appeared as a heterogeneous hypoechoic lesion with an unclear border in which the middle hepatic vein was seen running through it in B-mode ultrasonography (Fig. 1a) and Doppler ultrasonography (EUB-8500; Hitachi Medical Corporation, Tokyo, Japan). An abdominal CT (LightSpeed VCT; GE Healthcare, Waukesha, WI, USA) showed a 28 mm-wide tumor with a lobulated edge, diffuse homogeneous enhancement in the early phase and persistent enhancement in the delayed phase of dynamic contrast imaging (Fig. 2a–c). Magnetic resonance imaging (MRI) (Magnetom Trio, A Tim System; Siemens Healthcare, Erlangen, Germany) showed low and high intensity nodules in T1 and T2 weighted imaging with fat suppression, respectively (Fig. 2d,e), with a capsule-like lesion having a mosaic pattern in early contrast enhancement and persistent enhancement in the delayed phase (Fig. 2f–i). The tumor showed no decrease in signal intensity in T2 weighted images by superparamagnetic iron oxide magnetic resonance imaging (SPIO-MRI) (Fig. 2j) and was seen as feeding from the hepatic artery (A8) in both angiography and CT during hepatic arteriography (CTA). It also had enhanced persistency in the equilibrium phase of angiography, and revealed a complete contrast defect in CT during arterial portography (CTAP) (Fig. 3). These findings suggested that the tumor was neither common HCC nor CCC. We next performed CEUS using harmonic ultrasound and a bolus injection of 0.015 mL/kg Sonazoid and found a more extensive tumor area than the area shown in B-mode ultrasound, that was diffusely and homogeneously enhanced from 10 to 40 s in the pure arterial phase. The lesion became progressively hypoechoic relative to the adjacent liver parenchyma during the portal vein and late phases (mixed vascular phase), and provided a contrast defect with unclear border in the postvascular Kupffer phase (Figure 1b–e).

The tumor invasively proliferated in a duct-like configuration without production of mucinous fluid in a

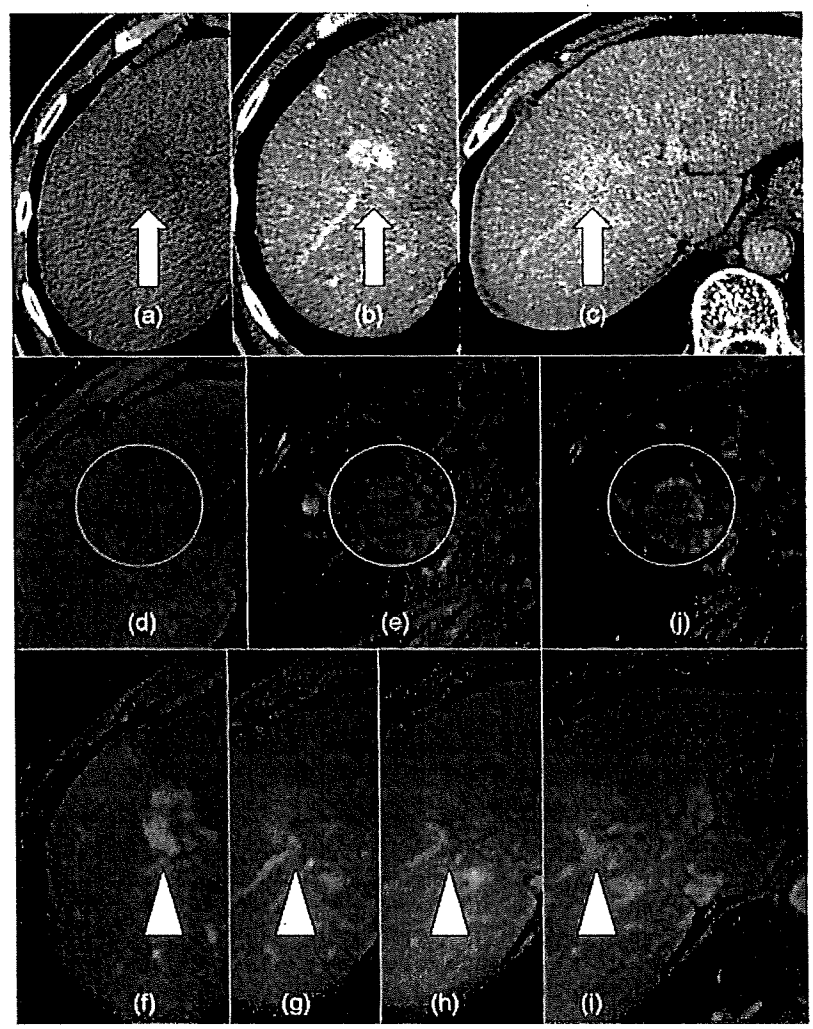

Figure 2 (a) Precontrast computed tomography (CT) depicted a hypoattenuating tumor (arrows) measuring 28 mm in diameter between the medial segment (S4) and anterior superior segment (S8) of the liver. (b) It showed enhancement in the early phase of dynamic enhanced CT. (c) It also showed persistent enhancement in the delayed phase. (d–e) Magnetic resonance imaging (MRI) showed low and high intensity nodules in T1 (d) and T2 (e) weighted imaging with fat suppression, respectively. (f–i) MRI revealed that the tumor (arrow heads) had mosaic pattern contrast enhancement in the early phase and persistent enhancement in the delayed phase: (f) 30 s, (g) 60 s, (h) 90 s, (i) 120 s after injection of contrast agent. (j) Superparamagnetic iron oxide MRI showed that the tumor had no decrease in signal intensity in T2 weighted images.

tissue specimen taken by ultrasound-guided biopsy. As the tumor had mild atypia, immunostaining of hepatocyte paraffin 1 (Hep par 1), cytokeratin (CK) 7, CK 19, epithelial membrane antigens (EMA) and neural cell adhesion molecule (NCAM) were negative, positive, slightly positive, strongly positive intraluminally but negative in the cytoplasm, and slightly positive, respectively. We thus histologically diagnosed the tumor as being well-differentiated CoCC. (Figure 4a–d)

The patient had a relative contraindication for surgical tumor resection because of the high risk of cerebrovascular complications due to cervical arteriosclerosis and his past history of asymptomatic lacunar infarction detected by brain MRI in preoperative analysis. The patient first opted for transcatheter arterial embolization (TAE), despite warnings that TAE might have no effect on this type of tumor. Indeed, no changes were seen one month later. After informing the patient about the risk of cerebrovascular complications of surgery, we obtained informed consent and performed an expanded anterior segmentectomy of the liver with lymph node dissection. The histological diagnosis after surgery was the same as the tumor biopsy.

DISCUSSION

THE CLINICAL AND imaging features of CoCC have not been fully characterized because only a small number of cases have been previously reported.[5,6,11–13] Most CoCC cases have hyper-enhancement in the early

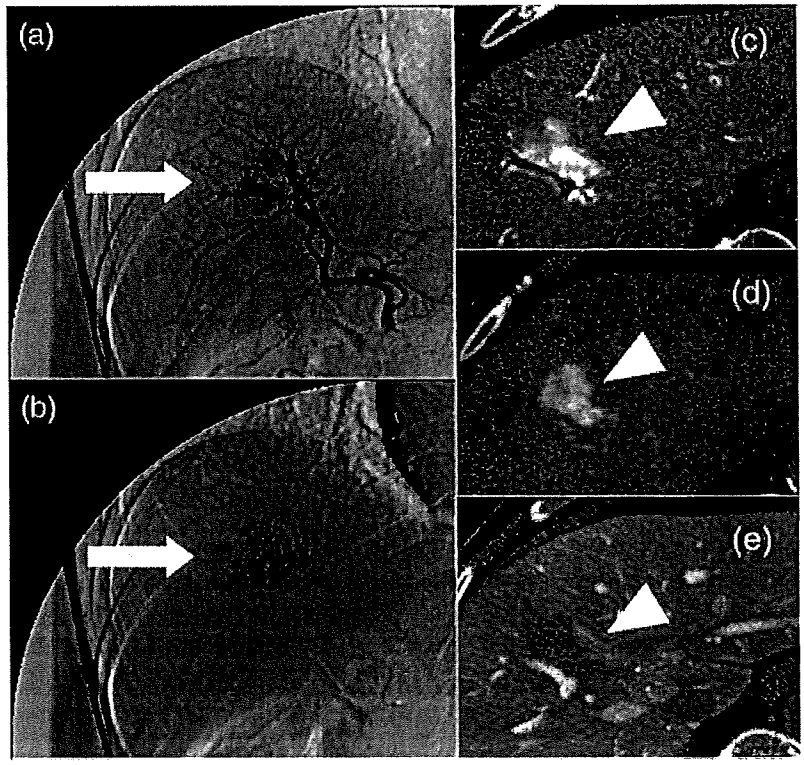

Figure 3 (a) Angiographic examination showed a hypervascular tumor (arrows) fed by the anterior superior branch of the right hepatic artery (A8). (b) The tumor had persistent enhancement in the equilibrium phase. (c) Computed tomography during hepatic arteriography (CTA) showed that the tumor (arrow heads) was enhanced. (d) Persistent enhancement was seen in the delayed phase. (e) It was depicted as a complete contrast defect by computed tomography during arterial portography (CTAP).

phase of contrast enhanced CT or MRI and hypervascularity in angiography.[6,13] Persistent enhancement in the late phase of contrast enhanced CT or MRI was also depicted in some cases,[5,6,11–13] reflecting slow diffusion of the contrast agent into the fibrotic component of the tumor similarly seen in cases with CCC.[14]

This study is the first to present findings of CoCC using ultrasonography with injection of Sonazoid. Sonazoid is a second-generation ultrasound contrast agent consisting of perfluorobutane gas microspheres stabilized by a membrane of hydrogenated egg phosphatidyl serine, which imparts more persistency in the bloodstream after injection than first-generation contrast agents.[15] In particular, Sonazoid enables stabilized images for more than 10 min after injection in the Kupffer phase, stemming from phagocytosis or trapping of the Sonazoid microspheres by Kupffer cells.[15,16] Thus, common HCC and other metastatic hepatic tumors present as contrast defect images in the Kupffer phase because they contain no Kupffer cells, unlike the surrounding hepatic parenchyma.[17,18] This was also the case in our patient; a contrast defect was seen in the Kupffer phase during CEUS.

In a report of overt HCC visualized using Sonazoid, a pure arterial supply was seen in the pure arterial phase, hypervascularity in the mixed vascular phase and a contrast defect in the Kupffer phase.[17] Similar characteristics in the arterial phase of this case were observed, in that we recognized the tumor with strongly homogeneous hyperperfusion, which was induced by blood pooling; assessment of microvessel density using immunohistochemical staining of the biopsy specimen for specific endothelial cell markers, such as CD 34,[19] showed an abundance of capillary endothelial vessels in the tumor (Figure 4e). In contrast, one report on common HCC using Sonazoid showed fast wash-out in the late vascular phase 3 minutes after injection of Sonazoid.[18] Visualization of CCC using Sonazoid has yet to be reported in the English literature. However, it has been reported using other second-generation contrast agents, and perfusion images of almost all cases revealed hyperperfusion in the arterial phase,[20,21] followed by punched-out contrast defects and relatively rapid wash-out in subsequent portal and/or sinusoidal phases.[20] The characteristics of this case in the mixed vascular phase are comparable to those of common HCC and CCC, in that

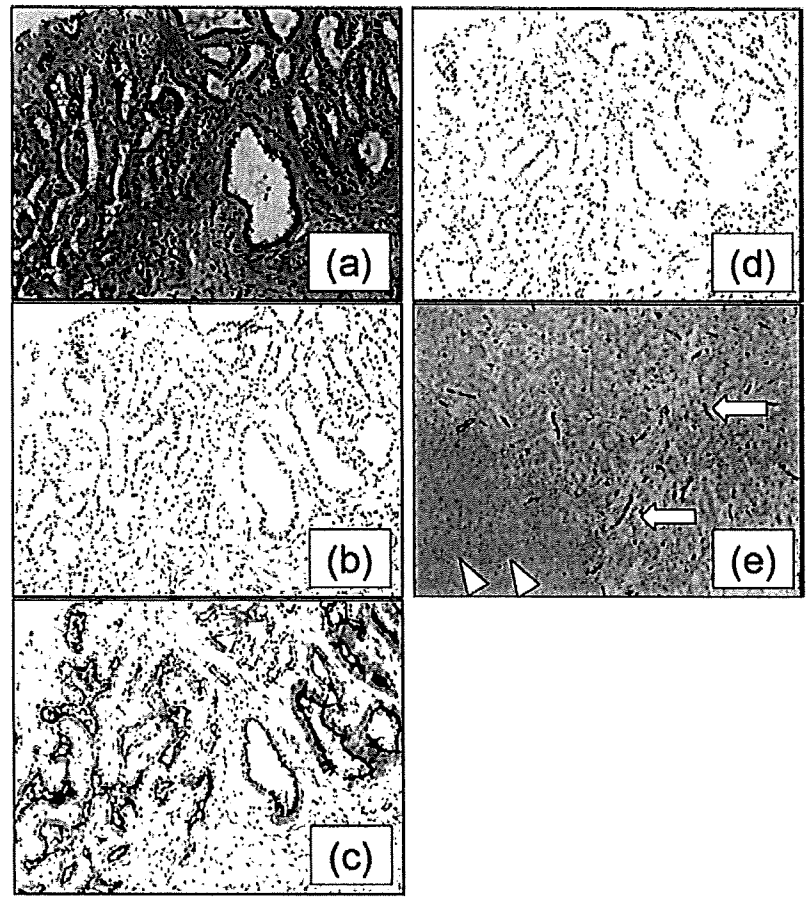

Figure 4 (a) Microscopic examination revealed that the tumor was a well-differentiated adenocarcinoma. The tumor was composed of small ovoid nuclei and eosinophilic cytoplasm with mild atypia and proliferated in an anastomosing pattern of Hering's canal-like small glands with fibrous stroma. We could not see production of mucinous fluid in ducts. Hematoxylin–eosin (HE) staining × 100. (b) Cells were immunohistologically negative to antibodies against hepatocyte paraffin 1 (Hep Par 1). × 100. (c) They also showed a strong intraluminal staining pattern of the gland for epithelial membrane antigens (EMA) × 100 (d) Cells were slightly positive for cytokeratin 19. (e) A number of capillary endothelial vessels stained with antibody for CD 34 antigens were seen in the cancerous part (arrows) compared to the non-cancerous part (arrowheads) × 25.

wash-out relatively early in the mixed vascular phase was described. We cannot generalize that all cases of CoCC show hyperperfusion in the arterial phase, relatively rapid wash-out in the mixed phase and complete contrast defect in the Kupffer phase because CoCC can show several pathologically different patterns.[22] Furthermore, more cases and comparisons with HCC and CCC are required to better characterize the images of CEUS with Sonazoid. Nonetheless, consideration of these CEUS findings should be helpful to elevate diagnostic accuracy in patients with CoCC.

In conclusion, our case of CoCC showed homogeneous hyperperfusion in the arterial phase, relatively rapid wash-out in the mixed vascular phase and then contrast defect with unclear border in the Kupffer phase using Sonazoid as a contrast agent. Clinicians should consider a hepatic tumor to be CoCC when the tumor simultaneously presents phenomena of both HCC and CCC in imaging tests. Incorporating findings from CEUS with those of CT, MRI and angiography will be helpful to better diagnose CoCC. Further studies are required to clarify the clinical and clinicopathological features of CoCC.

ACKNOWLEDGEMENT

WE THANK TREVOR Ralph for his editorial assistance.

REFERENCES

1 Steiner PE, Higginson J. Cholangiolocellular carcinoma of the liver. *Cancer* 1959 Jul–Aug; 12: 753–9.
2 Theise ND, Saxena R, Portmann BC *et al.* The canals of Hering and hepatic stem cells in humans. *Hepatology* 1999 Dec; 30: 1425–33.
3 Hirohashi S, Ishak K, Kojiro M, Wanless I, Theise N, Tsukuma H. Tumours of the liver and intrahepatic bile

ducts. In: Hamilton SR, Aaltonen LA, eds. *Pathology and Genetics of Tumours of the Digestive System*. Lyon: International Agency for Research on Cancer (IARC) Press, 2000; 257–02.
4 Japan LCSGO. *The General Rules for the Clinical and Pathological Study of Primary Liver Cancer*. Tokyo: Kanehara & Co., Ltd, 2008.
5 Shiota K, Taguchi J, Nakashima O, Nakashima M, Kojiro M. Clinicopathologic study on cholangiolocellular carcinoma. *Oncol Rep* 2001 Mar–Apr; 8: 263–8.
6 Kanamoto M, Yoshizumi T, Ikegami T *et al.* Cholangiolocellular carcinoma containing hepatocellular carcinoma and cholangiocellular carcinoma, extremely rare tumor of the liver: a case report. *J Med Invest* 2008 Feb; 55: 161–5.
7 Quaia E, Calliada F, Bertolotto M *et al.* Characterization of focal liver lesions with contrast-specific US modes and a sulfur hexafluoride-filled microbubble contrast agent: diagnostic performance and confidence. *Radiology* 2004 Aug; 232: 420–30.
8 Minami Y, Kudo M, Chung H *et al.* Contrast harmonic sonography-guided radiofrequency ablation therapy versus B-mode sonography in hepatocellular carcinoma: prospective randomized controlled trial. *AJR Am J Roentgenol* 2007 Feb; 188: 489–94.
9 Numata K, Morimoto M, Ogura T *et al.* Ablation therapy guided by contrast-enhanced sonography with Sonazoid for hepatocellular carcinoma lesions not detected by conventional sonography. *J Ultrasound Med* 2008 Mar; 27: 395–406.
10 Forsberg F, Piccoli CW, Liu JB *et al.* Hepatic tumor detection: MR imaging and conventional US versus pulse-inversion harmonic US of NC100100 during its reticuloendothelial system-specific phase. *Radiology* 2002 Mar; 222: 824–9.
11 Yamamoto M, Takasaki K, Nakano M, Saito A. Hepatic recurrence of cholangiolocellular carcinoma: report of a case. *Hepatogastroenterology* 1996 Jul–Aug; 43: 1046–50.
12 Fukukura Y, Hamanoue M, Fujiyoshi F *et al.* Cholangiolocellular carcinoma of the liver: CT and MR findings. *J Comput Assist Tomogr* 2000 Sep–Oct; 24: 809–12.
13 Matsuda M, Hara M, Suzuki T, Kono H, Fujii H. Synchronously resected double primary hepatic cancers – hepatocellular carcinoma and cholangiolocellular carcinoma. *J Hepatobiliary Pancreat Surg* 2006; 13: 571–6.
14 Lacomis JM, Baron RL, Oliver JH, 3rd, Nalesnik MA, Federle MP. Cholangiocarcinoma: delayed CT contrast enhancement patterns. *Radiology* 1997 Apr; 203: 98–104.
15 Sontum PC. Physicochemical characteristics of Sonazoid, a new contrast agent for ultrasound imaging. *Ultrasound Med Biol* 2008 May; 34: 824–33.
16 Yanagisawa K, Moriyasu F, Miyahara T, Yuki M, Iijima H. Phagocytosis of ultrasound contrast agent microbubbles by Kupffer cells. *Ultrasound Med Biol* 2007 Feb; 33: 318–25.
17 Kudo M. New sonographic techniques for the diagnosis and treatment of hepatocellular carcinoma. *Hepatol Res* 2007 Sep; 37 (Suppl 2): S193–9.
18 Hatanaka K, Kudo M, Minami Y *et al.* Differential diagnosis of hepatic tumors: value of contrast-enhanced harmonic sonography using the newly developed contrast agent. *Sonazoid. Intervirology* 2008; 51 (Suppl 1): 61–9.
19 Sasano H, Suzuki T. Pathological evaluation of angiogenesis in human tumor. *Biomed Pharmacother* 2005 Oct; 59 (Suppl 2): S334–6.
20 Celli N, Gaiani S, Piscaglia F *et al.* Characterization of liver lesions by real-time contrast-enhanced ultrasonography. *Eur J Gastroenterol Hepatol* 2007 Jan; 19: 3–14.
21 Dietrich CF. Characterisation of focal liver lesions with contrast enhanced ultrasonography. *Eur J Radiol* 2004 Jun; 51 (Suppl): S9–17.
22 Komuta M, Spee B, Vander Borght S *et al.* Clinicopathological study on cholangiolocellular carcinoma suggesting hepatic progenitor cell origin. *Hepatology* 2008 May; 47: 1544–56.

Liver International ISSN 1478-3223

CLINICAL STUDIES

Phylogenetic analysis of hepatitis A virus in sera from patients with hepatitis A of various severities

Keiichi Fujiwara[1], Hiroshige Kojima[1], Yutaka Yonemitsu[1], Shin Yasui[1], Fumio Imazeki[1], Makoto Miki[2], Kazuyuki Suzuki[3], Isao Sakaida[4], Kiwamu Okita[4], Eiji Tanaka[5], Masao Omata[6] and Osamu Yokosuka[1]

1 Department of Medicine and Clinical Oncology, Graduate School of Medicine, Chiba University, Chiba, Japan
2 Department of Internal Medicine, Yokohama Higashi National Hospital, Kanagawa, Japan
3 First Department of Internal Medicine, Iwate Medical University, Iwate, Japan
4 Department of Gastroenterology and Hepatology, Yamaguchi University School of Medicine, Yamaguchi, Japan
5 Department of Medicine, Shinshu University School of Medicine, Nagano, Japan
6 Department of Gastroenterology, Faculty of Medicine, University of Tokyo, Tokyo, Japan

Keywords
2B – 2C – 5′NTR – fulminant hepatitis – hepatitis A – hepatitis A virus

Abbreviations
AH, acute hepatitis; AHs, acute hepatitis severe type; FH, fulminant hepatitis; HAV, hepatitis A virus; PT, prothrombin time.

Correspondence
Keiichi Fujiwara, MD, PhD, Department of Medicine and Clinical Oncology, Graduate School of Medicine, Chiba University, 1-8-1 Inohana, Chuo-ku, Chiba 260-8670, Japan
Tel: +81 43 226 2083
Fax: +81 43 226 2088
e-mail: fujiwara-cib@umin.ac.jp

Received 13 August 2008
Accepted 4 October 2008

DOI:10.1111/j.1478-3231.2008.01919.x

Abstract

Background: We analysed the association of the 5′ nontranslated region (5′NTR), nonstructural proteins 2B and 2C of the hepatitis A virus (HAV) genome, whose mutations have previously been shown to be important for enhanced replication in cell culture systems, in order to align all our data and examine whether genomic differences in HAV are responsible for the range of clinical severities. *Methods:* Our accumulated HAV strains of 5′NTR [nucleotide(nt) 200 and 500], entire 2B and 2C from 25 Japanese patients with sporadic hepatitis A, consisting of seven patients with fulminant hepatitis (FH), five with severe acute hepatitis (AHs) and 13 with self-limited acute hepatitis (AH), in whom the sequences of all three regions were available, were subjected to phylogenetic analysis. *Results:* Fulminant hepatitis patients had fewer nucleotide substitutions in 5′NTR, had a tendency to have more amino acid (aa) substitutions in 2B and had fewer aa substitutions in 2C than AH patients. Four FH and two AHs with a higher viral replication were located in the near parts of the phylogenetic trees, indicating the association between the severity of hepatitis A and genomic variations in 5′NTR, 2B and 2C of HAV. *Conclusions:* Our study suggests that genetic variations in HAV not in one specific region but in 5′NTR, 2B and 2C might cooperatively influence replication of the virus, and thereby affect virulence. Viral factors should be considered and examined when discussing the mechanisms responsible for the severity of hepatitis A.

Hepatitis A is still a major problem worldwide, not only in underdeveloped countries but also in industrialized nations. Because of improvements in sanitation, there have been no hepatitis A epidemics in Japan in recent years. However, sporadic cases of hepatitis A have not been rare of late. Although the majority of hepatitis A cases are self-limited acute hepatitis (AH), some develop into severe forms of hepatitis (1). In fact, in the past several years, there has been an increase in the numbers of patients with sporadic hepatitis A, especially the more severe kind, visiting our hospital. Our analysis of the possible factors responsible for the disease severity in our patients revealed no significant differences in terms of background including age, suggesting that viral factors might be involved in determining the severity of the disease (2, 3).

Hepatitis A virus (HAV) is the sole member of the hepatovirus genus and a member of the Picornavirus family. Virological studies have revealed that HAV is a positive-strand RNA virus comprising approximately 7500 nucleotides and containing a 5′ nontranslated region (NTR), a single long open reading frame encoding a large polyprotein and a 3′NTR. A large polyprotein is cleaved by the viral protease to produce the P1, P2 and P3 regions. The P1 region encodes four structural proteins – VP4, VP2, VP3 and VP1. The P2 and P3 regions encode nonstructural proteins 2A, 2B and 2C, and 3A, 3B, 3C and 3D respectively (4). As far as is known, nonstructural protein 2A participates in virion morphogenesis (5). 2B and 2C play important roles in the replication of viral RNA. 2C is a multifunctional protein and is considered to have helicase and NTPase activities. 2C or 2BC have membrane- and RNA-binding properties (6). 3B is considered to be a genome-linked viral protein (Vpg), 3A a pre-Vpg, 3C a viral protease and 3D an RNA-dependent RNA polymerase.

It was reported that the strains adapted to cell culture systems have mutations in 5′NTR and the P2 region of HAV (7, 8). Zhang *et al.* (9) reported that rapidly replicating, cytopathic variants of HAV isolated from cultured cells required mutations within 5′NTR, 2B and 2C, and these mutations acted cooperatively. Raychaudhuri *et al.* (10) reported that the simian virus 2C gene could confer the phenotype of virulence to an otherwise attenuated virus, and clusters of residues near both ends of the 2C protein were required for virulence using chimeras between human and simian strains of hepatitis A virus in tamarins.

Despite advances in the understanding of HAV, a correlation between the HAV genome and the clinical status of hepatitis A has not been established. Durst *et al.* (11) reported a cluster of fulminant hepatitis A, in which the severity of the infection in three siblings was related to the virulence of HAV. To examine the possibility of differences in hepatitis A viruses in terms of the different categories of hepatitis, we have analysed the viral genomes in sera from hepatitis A patients with a variety of clinicopathological features and reported the associations between some viral regions and clinical severities (3, 12–18).

When analysing the viral genome, rather than focusing on one specific region, perhaps several portions of the HAV genome should be investigated. In the present study, we examined the clinicopathological features of hepatitis A and possible correlations with variations in the three regions of 5′NTR, 2B and 2C of the HAV genome, whose mutations have previously been shown to be important for enhanced replication and virulence in cell culture systems and simians, in the same patients using phylogenetic analysis.

Materials and methods

Patients

Serum samples from 25 patients with hepatitis A in Japan were collected between 1986 and 1999 and stored at −20 °C until analysis. Informed consent was obtained from the patients or appropriate family members. These patients were diagnosed based on the positivity of the IgM antibody to HAV (IgM anti-HAV) in conjunction with compatible symptoms and laboratory findings.

Among the patients seven had fulminant hepatitis (FH), five had severe acute hepatitis (AHs) and 13 had self-limited AH. Patients with a prothrombin time < 40% of control were defined as AHs, and those with hepatic encephalopathy as FH. Patients with significant increases in serum blood urea nitrogen and creatinine (more than three times the upper level of the normal range) were judged to be undergoing acute renal failure. The patients were also investigated for histories of recent exposure to drugs and chemical agents as well as heavy alcohol consumption (> 50 g/day for > 5 years).

None of the patients had clinical or laboratory evidence of acquired immune deficiency syndrome.

Serological markers

IgM antibody to HBc(IgM anti-HBc), HBsAg and second-generation antibody to hepatitis C virus (HCV) were examined in all cases. IgM anti-HAV, IgM anti-HBc and HBsAg were measured by commercial radioimmunoassay kits (Abbott Laboratories, Chicago, IL, USA); second-generation HCV antibody was measured by the enzyme immunoassay kit (Ortho Diagnostics, Tokyo, Japan). In the FH and AHs patients, HCV RNA, IgM antibody to Epstein–Barr virus (IgM anti-EBV), IgM antibody to herpes simplex virus (IgM anti-HSV), IgM antibody to cytomegalovirus (IgM anti-CMV), anti-smooth muscle antibody, liver kidney microsomal antibody-1 and anti-mitochondrial antibody were also examined. HCV RNA was measured by nested reverse transcriptase-polymerase chain reaction (RT-PCR) as described by the authors (19). IgM anti-EBV, IgM anti-CMV and IgM anti-HSV were examined by enzyme-linked immunosorbent assays. Anti-nuclear antibody, anti-smooth muscle antibody, anti-mitochondrial antibody and anti-liver kidney microsomal-1 antibody were examined by the fluorescent antibody method.

Quantification of hepatitis A virus RNA by real-time reverse transcriptase-polymerase chain reaction

Serum viral RNA was extracted by the High Pure Viral RNA Kit (Roche Diagnostics GmbH, Mannheim, Germany). RT-PCR was carried out with a Hepatitis A Virus Quantification Kit (Roche Diagnostics) according to the manufacturer's instructions. Twenty microliters of the PCR mixture contained 15 μl of master mix from the kit and 5 μl of template RNA. The standards of HAV RNA are supplied with this kit. All reactions were performed in a LightCycler (Roche Diagnostics). The C_T values from clinical samples were plotted on the standard curve, and the number of copies wes calculated automatically. This method has a dynamic range of HAV RNA quantification between 0.5 and 5×10^6 copies/μl.

Amplification of serum hepatitis A virus RNA and direct sequencing

Hepatitis A virus RNA was examined by nested RT-PCR and direct sequencing as described previously (14, 17, 18).

Nucleotide sequence accession numbers

The nucleotide sequence data reported herein appear in DDBJ/EMBL/GenBank nucleotide sequence databases with the following accession numbers:

5′NTR

AB045327 for A1, AB045336 for A5, AB045330 for A204, AB045331 for A205, AB045332 for A206, AB045334 for A414, AB045338 for A601, AB045342 for A159, AB045344 for A160, AB045345 for A161, AB045350 for A302, AB045353 for A811, AB045672 for A7, AB045692